Microstructural characterization of high-silicon iron alloys produced by spray forming and co-injection of Si particles

R.D. Cava [a], D.P. Oliveira [a], T. Yonamine [c], J.J.A. Moreira [b], W.J. Botta [b], C.S. Kiminami [b,*], C. Bolfarini [b]

[a] Post-Graduate Program in Materials Science and Engineering, Federal University of São Carlos, São Carlos, SP, Brazil
[b] Department of Materials Engineering, Federal University of São Carlos, São Carlos, SP, Brazil
[c] Inmetro – Dimci/Dimat – National Institute of Metrology Standardization and Industrial Quality, SP, Brazil

ABSTRACT

Fe–Si alloys are widely used for magnetic applications. However, it is very difficult to process Fe–Si with a silicon content exceeding 3.5 wt.%Si (upper limit for products commercially available by the I/M route) due to the alloy's low ductility, which is attributed mainly to the formation of B2 and DO3 ordered phases that embrittle the material. To overcome this obstacle, the main focus of this work is to produce thin sheets of Fe–5 wt.%Si alloy in two steps: (1) as a Fe–3.5%Si + 3%Si_p (Si particles) composite, using spray forming, and (2) rolling and heat treating (HT) the composite to dissolve the silicon and homogenize its content throughout the thickness of the sheet. To this end, 3 wt.%Si_p were co-injected into the main stream of the Fe–3.5 wt.%Si spray, followed by hot-rolling of the billet at 850 °C to obtain 0.45 mm gauge thin sheets. The final material was heat-treated at 780/510 °C for 8 h or at 1250 °C for 1 h and then air cooled. The grain orientation was analyzed by EBSD and the distribution of iron, silicon and impurities was identified by X-ray dot mapping. The heat treatment caused diffusion and dissolution of the silicon particles and grain growth. However, the final silicon content was strongly dependent on the atmosphere of the heat treatment furnace. In the absence of oxygen, the silicon content reached 4.9 wt.% distributed homogeneously throughout the thickness of the composite. In the presence of oxygen, the silicon diffused to the surface and only 3.5 wt.% remained in the matrix.

© 2011 Elsevier B.V. All rights reserved.

1. Introduction

The addition of silicon to iron improves the latter's magnetic properties by increasing the material's electrical resistivity and decreasing its magnetic anisotropy constant and magnetostriction [1]. However, at concentrations above 3.5 wt.%, silicon strongly decreases the ductility of Fe–Si alloys, rendering the material too brittle to be cold or hot-rolled without cracking during the production of thin sheets for electromagnetic applications [2]. Therefore, commercial silicon–iron sheets have a maximum Si content of approximately 3.5 wt.% [3].

Rapid solidification processes have been used to produce Fe–6.5 wt.%Si alloys directly from the melt [4,5]. The product of the melt-spinning process is a microcrystalline ribbon with improved ductility, which can be bent and cold-rolled. In the as quenched state, the magnetic properties of the ribbons are poor and grain orientation is random. The low magnetic loss in the longitudinal direction of the ribbon is attributed to the inherent texture of the material after heat treatments. However, the high cost of melt-spinning processing is a drawback for the use of this route for the production of thin sheets for electromagnetic applications.

The spray-forming process is a variant of rapid solidification processes and is based on the atomization of a liquid metal stream by an inert gas [6]. In this process, atomized droplets are consolidated into a dense deposit on a substrate. By controlling the relative movement between the spray and the substrate, simple geometrical shapes such as bars, sheets and tubes can be produced directly from the melt. Grain size and orientation are crucial for the improvement of the magnetic properties and are closely related to process parameters, including heat treatments.

Our previous papers reported that the grain size in spray cast deposits is determined by the conditions of the spray upon impact, the spatial distribution of solid particles after impact, the time required for complete solidification and the cooling rate after solidification [7,8]. Moreover, the magnetic properties of Fe–Si alloys are affected by order–disorder transitions, a dependence that has been investigated by several authors [9,10]. Despite the refined and very homogeneous microstructure, spray-formed deposits are still difficult to be hot/cold-rolled due to the A2-disordered/B2-ordered transformation occurring at about 973 K in Fe–6.5 wt.%Si alloys [11]. Our group investigated the possibility of keeping the A2-disordered phase metastable at a temperature below 973 K by

* Corresponding author.
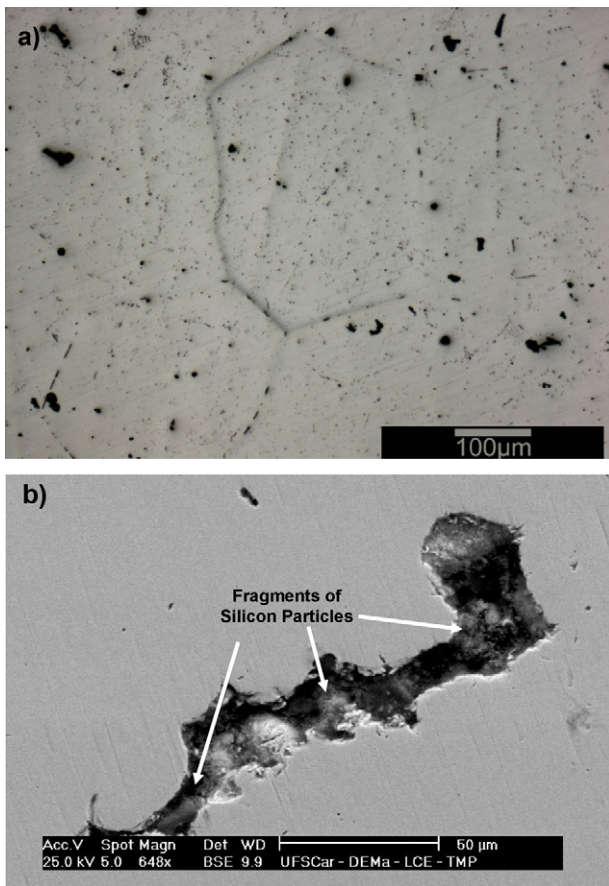 E-mail address: kiminami@ufscar.br (C.S. Kiminami).

Fig. 1. Microstructures by Optical and SEM/BSE mode of the deposit showing: (a) equiaxial grains and micropores; (b) "pullout porosity" containing fragments of co-injected particles.

Fig. 2. Sheet microstructures after rolling: (a) surface; (b) cross section.

adding Al to spray-formed deposits of Fe–Si alloys, which could allow these deposits to be rolled without cracking. However, the addition of aluminum to the alloy leads to the formation of inclusions that impair its magnetic properties [12,13]. Therefore, our efforts focused on the fabrication of an Al-free alloy. To overcome the problem of ductility, the Fe–6.5 wt.%Si alloy was developed as a composite: Fe–3.5%Si + 3%Si$_p$ produced by spray forming. This paper describes the microstructure and characterization of the spray-formed Fe–3.5 wt.%Si + 3 wt.%Si$_p$ composite.

1.1. Experimental procedures

Approximately 5 kg of Fe–3.5 wt.%Si alloy was prepared from electrolytic iron and silicon (99.9% purity) by induction melting in an alumina crucible under an argon atmosphere. The molten alloy was superheated to 1650 °C and then, delivered through a quartz pouring tube and atomized by nitrogen in a static close-coupled atomizer. Gas pressure was set to obtain a gas-to-metal mass flow ratio, GMR, of 0.12. Simultaneously, 3 wt.% of commercial silicon particles in the range of 106–250 μm were incorporated into the atomized spray through an injector, using nitrogen under a pressure of 0.20 MPa. The flight or spray distance was adjusted to 350 mm and the atomized metallic droplets and co-injected particles were deposited onto a 1020 steel substrate rotating at 60 rpm. The equipment used to produce the deposits was described elsewhere [7]. Nitrogen of 99.99% purity was used for atomization. Specimens with dimensions of 70 mm × 30 mm × 5.2 mm were machined out from the center of the deposit, reheated at 850 °C for 5 min, and warm rolled in FENN model 051 rolling mill to a final thickness of 0.45 mm, corresponding to a total reduction in thickness of 91.3%. After the rolling process, two heat treatments were performed as follows. Treatment (1): annealing and grain growth heat treatments at 780 °C for 6 h and iron oxidation surface treatment for another 2 h at 510 °C in an H$_2$/H$_2$O atmosphere with controlled humidity and furnace cooling. Treatment (2): annealing at 1250 °C for 1 h in a vacuum-sealed quartz tube with approximately 3 g Ti (99.99% purity) and air cooling. The microstructures and grain size of the deposits and rolled materials were examined under an Olympus BX2 series optical microscope and the microstructure, chemical distribution of iron, silicon, carbon and oxygen elements
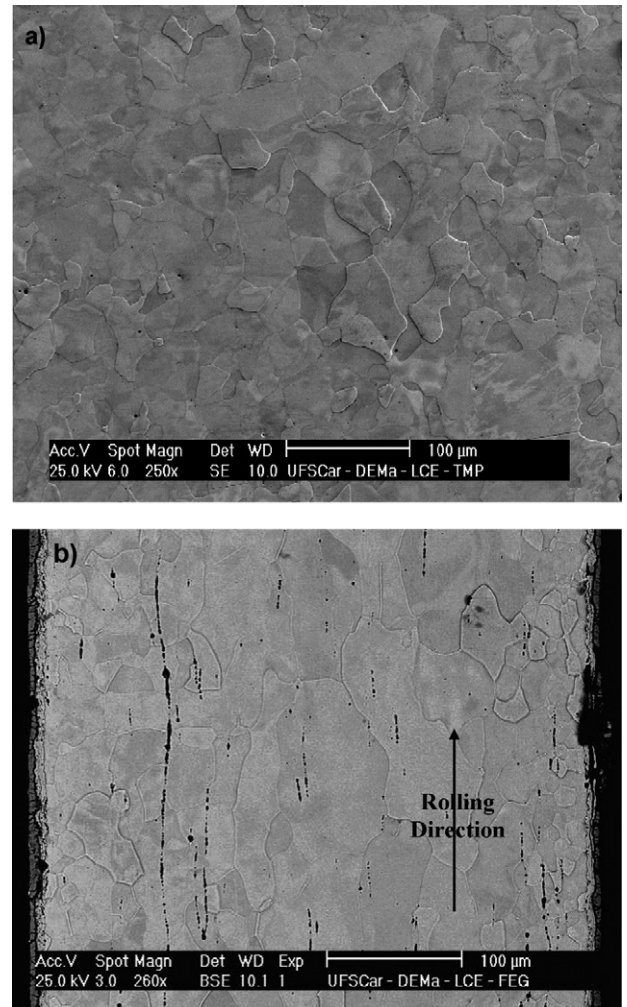
and the texture were analyzed using a Philips XL30-FEG-SEM microscope equipped with an Oxford Link ISIS 300 EDS spectrometer and a TSL EBSD diffractometer. The microhardness of all the materials was determined. After Heat Treatment (2), the chemical distribution of elements was also identified by X-ray dot mapping of the laminated material to ascertain the effect of the heat treatment on silicon diffusion.

2. Results and discussion

The SEM/EDS images of the matrix alloy and particles of the composite revealed chemical compositions of 96.41 wt.%Fe, 3.52 wt.%Si and 0.07 wt.%O in the matrix, and 26.91 wt.%Fe, 72.68 wt.%Si, 0.33 wt.%Ca and 0.04 wt.%Al in the particles. It should be noted that the final chemical composition of the deposit attained a maximum mean value of Fe5.8 wt.%Si. For the deposit, this indicates a low yield (−66% in wt.%Si$_p$) produced by the co-injection system, using the aforementioned processing parameters.

Fig. 1 shows the microstructures of the deposit. Note the equiaxial grains and heterogeneous distribution of the particles in the matrix. Fig. 1(b) shows no evidence of dissolution of the silicon particles during the atomization process, since SEM/EDS analyses of the matrix adjacent to particles showed the same composition as that of the matrix in the region without silicon particles. In addition, the chemical composition in regions containing particles (Fig. 1(b)) showed 17.81 wt.%Si, and 74.72 wt.%Fe, as well as 7.47 wt.% of impurities (3.47 wt.% calcium, 1.54 wt.% aluminum and 2.36 wt.% oxygen). This indicates that the amount of silicon detected in the
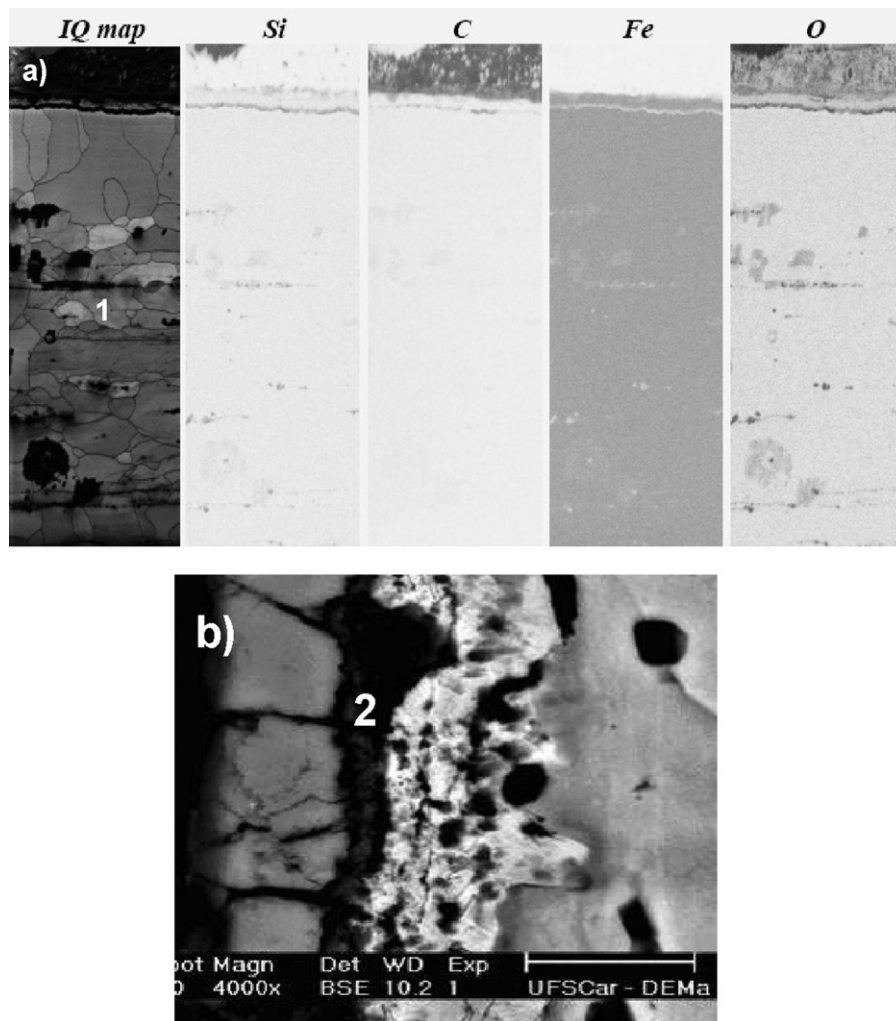
Fig. 3. Heat-treated microstructures. (a) Microstructure and X-Ray dot mapping of the longitudinal section of the thin sheet after Heat Treatment (1); (b) detail of surface oxidation (point 2).

analysis was influenced by the matrix (17.81 wt.%Si analyzed vs. 72.68 wt.%Si inserted particles) and the impurities, although a high content of this element was detected. It is likely that the silicon element of the particles inserted during the process did not undergo dissolution or major diffusion. Moreover, all the material clearly shows the presence of microporosity (Fig. 1(a)). Although no macropores were observed, particle pullout during preparation of the samples made it difficult to differentiate between porosity and pullout. Point-by-point analysis by SEM/EDS was therefore used in this case. The porosity levels of the alloys were calculated using density values obtained by the Archimedes method. The porosity results showed a mean volumetric value of 2.01% for the different regions, except for a 2 mm thick region at the bottom of the deposit, where porosity was considerably higher and was therefore not considered in the measurements.

Fig. 2 shows the typical microstructures of the thin sheets after warm rolling. The grains are partially recrystallized, albeit only at the surface. In the central region of the sheet, the grains showed no evidence of recrystallization, retaining the partially elongated shape assumed during rolling. Stringers of broken silicon particles are also visible, indicating that the rolling process led to a strong decrease in the mean particle size and to heterogeneous particle distribution. Moreover, note that the particles were not dissolved during the rolling process, showing that the available energy was insufficient to promote particle dissolution.

Fig. 3 shows images of the microstructure in cross section captured by SEM–EDS and the X-ray dot mapping to verify the distribution of Fe, Si and O through the thickness of the sheet heat-treated by Treatment (1). Due to the relatively low temperatures employed, the material underwent minor grain growth only adjacent to the surface (point 1, Fig. 3(a)), while the grains inside the sheet remained non-recrystallized (Fig. 3(b)), indicating that more energy for recrystallization was available close to the surface. This result was expected, since in high silicon alloys recrystallisation is influenced by ordering reactions; below a critical ordering temperature the structure is characterised by domains, with a high degree of order separated by the anti-phase boundary (APB). These regions have a critical importance on the deformation and annealing behaviour [14]. Therefore, at the temperature of the annealing heat treatment employed, 780 °C, the recrystallisation was retarded due to the high degree of order which should be still retained at this temperature for this silicon content [15]. Moreover, undissolved silicon particles remained present in the matrix of the specimen. SEM/EDS analyses indicated a considerable difference in silicon content: 3.51 wt.%Si – point 2, central region (see Fig. 3(b)) – and 41.61 wt.%Si – point 3, peripheral region (see detail in Fig. 3(a)). It appears that the presence of oxygen inside the furnace strongly influenced the diffusion of silicon towards the surface, as driving force free the enthalpy of formation of silicon oxide. This resulted in silicon impoverishment in the central regions of the sheet, pre-
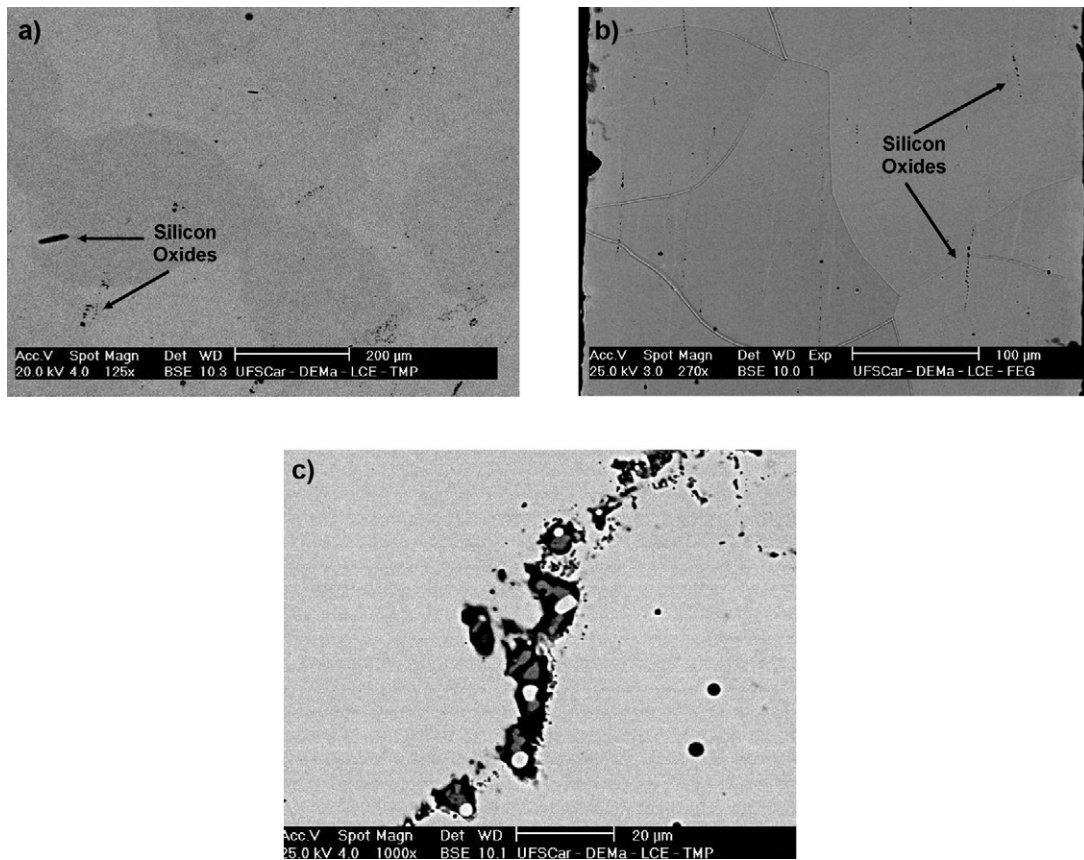
Fig. 4. (a and b) Surface and longitudinal cross sections of the microstructures of the rolled material after Treatment (2); (c) string of silicon oxide inclusions from the powder used for co-injection of the silicon particles. Even the heat treatment at 1250 °C during heat Treatment (2) did not alter its configuration.

cluding the desired high level of silicon content homogeneously dissolved in the matrix and formation of the ordering phase. The X-ray dot map clearly shows oxidation of the remaining undissolved particles, which can be identified as silicon oxide inclusions, and a strong concentration of silicon at the surface, indicating the effect of the oxidation process on silicon diffusion. It should also be noted that the scanty presence of silicon concentrations through the thickness of the sheet was consistently associated with the presence of oxygen, implying that part of the co-injected particles were already present as silicon oxide, which can explain the non-dissolution of these particles. Despite the fact that the presence of these oxide inclusions did not impair the rolling operation, better raw material must be selected for the co-injection process in order to achieve the desired silicon content and to avoid the detriment in the magnetic properties.

Treatment (1) was chosen in order to allow the use of an industrial facility dedicated for the production of electrical compliances with conventional electrical steel (low silicon content) to evaluate the possibility of using the same equipment for the high silicon alloy, which would make easier the introduction of this alloy type in the industry. However, the results of this work pointed out clearly that a higher temperature and a protective atmosphere must be used when working with high silicon electrical steels in order to avoid silicon loss and to promote total recrystallization and grain growth.

The high-temperature heat treatment, Treatment (2), at 1250 °C for 1 h under vacuum, enabled total grain recrystallization, including strong grain growth (Fig. 4). Similar to the results of Treatment (1), the silicon oxide particles remained undissolved in the microstructure of the matrix. However, in this case, due to the protection provided by the vacuum during the heat treatment and the

Table 1
Vickers hardness in all the conditions.

Sample	Rolled	Treatmt. (1)	Treatmt. (2)
Condition	WH	PR	TR
%Si (wt)	5.32	3.39	4.90
Mean	256.60	186.0	218.0

WR: warm rolling; PR: partial recrystallization, and TR: total recrystallization.

presence of titanium, the silicon did not migrate towards the surface and its content showed a mean value of 4.9 wt.% distributed homogeneously through the thickness. It is probable that the target content of 6.5 wt.%Si was not attained due to the poor yield of the co-injection system used for deposition and the use of Si powder containing some silicon oxide instead of only Si particles.

Tables 1 and 2 describe the Vickers hardness and grain size, respectively, of the materials under study. A comparison of the rolled condition with that of Treatment (1) indicates that minor grain growth occurred (14.2 ± 1.2 to 56.5 ± 4.5) and that the hardness decreased in response to the partial recrystallization process during the heat treatment. In this condition, the energy applied to the material in Treatment (1) was insufficient to promote diffusion of the silicon. The higher temperature employed in Treatment

Table 2
Grain size of all the materials at work.

Sample (condition)	%Si (wt)	Surface	
Rolled (WR)	5.32	14.2	± 1.2
Heat (1) (PR)	3.39	56.5	± 4.7
Heat (2) (TR)	4.90	235.1	± 32.4

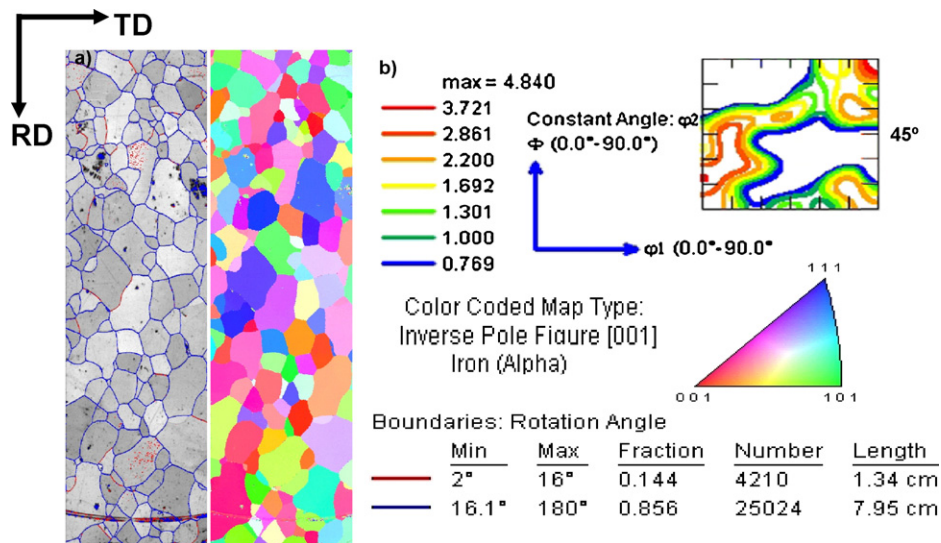WR: warm rolling; PR: partial recrystallization, and TR: total recrystallization.

Fig. 5. (a) EBSD image; (b) $\varphi 2 = 45°$ ODF section.

(2) promoted total recrystallization and a strong grain growth (14.2 ± 1.2 to 235 ± 32). Despite this the hardness increased. This apparently conflicting result can be explained by the higher silicon content resulting from the application of this heat treatment, which at this level, i.e., 4.9 wt.%Si, may lead to the formation of DO3 and B2 ordered phases, and therefore to increased hardness. EBSD analyses of the sheets heat-treated by Treatment (2) were performed to evaluate the possible development of Goss texture due to the presence of particulate material in the rolling step. Fig. 5 shows the grain orientation resulting from rolling in the longitudinal direction. Particular mention should be made to the RD (rolling direction) and ND (normal direction) fibers because they contain most of the important orientations in cold-rolled and annealed steels. These fibers are composed of groups of orientations whose $\langle 1\,1\,0 \rangle$ axis is parallel to the RD in the former case, or the $\langle 1\,1\,1 \rangle$ axis parallel to the ND in the latter case. Fig. 5(a) shows recrystallized grains and grain growth after heat treatment, with Si particles almost completely dissolved in the matrix. As seen in Fig. 5(b), the final texture tends toward the Goss direction $\{0\,1\,1\}\langle 1\,0\,0 \rangle$, which is visible in this composite after annealing and is associated with nucleation of the desirable texture component. However, there is no preferential orientation and the texture is random, leading us to conclude that the presence of the particles did not affect the development of the texture. We had already obtained the same result in a previous work by rolling Fe–Si alloys without particle co-injection [16]. Other authors pointed out similar difficulties to establish a strong Goss texture by working with high silicon electrical steels, the main reason being the brittleness of the alloys that hinders the final cold rolling operation before annealing heat treatment [17–19], even using very complex rolling steps. Directional recrystallization, a process where the material is annealed by passing it through a strong temperature gradient, can produce columnar grains presenting crystallographic texture [20,21]. More recently, Zhang et al. [22] employed this technique in an Fe–6.5 wt.%Si alloy and claimed to obtain a strong crystallographic texture, which resulted in a reduction of the alloy's coercivity for a very well defined direction (in other directions a worsening of the coercivity was measured). However, these authors used thicker (1.5 mm against 0.45 mm in our work) and very small samples to get these results, remaining an open question whether these results could be useful for real materials.

In order to prevent cracking by rolling Fe–6.5 wt.%Si alloys several methods have been reported in the literature, such as surface diffusion, chemical vapour deposition (CVD) [23] and a hot dipping process followed by diffusion annealing [24]. However, these processes resulted in expensive materials with inexpressive market share. The processing route displayed in this work proved to allow the fabrication of the thin sheets of high silicon iron alloys in a quite straight forward way without cracking the brittle material. However, high temperature annealing heat treatment is necessary for recrystallization and grain growth.

3. Conclusions

The production of composite material with co-injection of silicon particles into the spray allowed the production of thin sheets of Fe–Si alloys with silicon content exceeding that of commercially available alloys.

Oxide particles break and do not present difficulties during rolling operations, but remain in the final microstructure and can impair the magnetic properties.

References

[1] R.M. Bozorth, Ferromagnetism: Iron–Silicon Alloys, first ed., Van Nostrand, New York, 1951.
[2] Y. Takada, M. Abe, S. Masuda, J. Inagaki, J. Appl. Phys. 64 (1988) 5367–5369.
[3] M.A. Cunha, G.W. Johnson, J. Mater. Sci. 25 (1990) 2481–2486.
[4] K.I. Arai, K. Ishyiama, J. Magn. Magn. Mater. 133 (1994) 233–237.
[5] X.F. Bi, K.I. Arai, IEEE Trans. Magn. 32 (1996) 4818–4820.
[6] A.R. Singer, Int. J. Powder Metall. Powder Technol. 21 (1985) 219–234.
[7] R.J. Santos, C. Bolfarini, C.S. Kiminami, Mater. Sci. Forum 299–300 (1999) 398–406.
[8] M.M. Pariona, C. Bolfarini, C.S. Kiminami, Metallkd 89 (1998) 494–498.
[9] D. Bouchara, M. Agot, J. Degauque, J. Bras, J. Magn. Magn. Mater. 83 (1990) 377–378.
[10] J. Degauque, D. Bouchara, M. Fagot, J. Bras, J.P. Redoules, P. Chomel, B. Astie, IEEE Trans. Magn. 26 (1990) 2220–2222.
[11] S. Matsumura, Y. Tanaka, Y. Koga, K. Oki, Mater. Sci. Eng. A 312 (2001) 284–292.
[12] A.H. Kasama, C. Bolfarini, C.S. Kiminami, W.J. Botta Filho, Mater. Sci. Eng. A 449–451 (2007) 375–377.
[13] C. Bolfarini, F. Audebert, W.J. Botta, C.S. Kiminami, F. Saporiti, A.H. Kasama, B. Arcondo, Mater. Sci. Forum 570 (2008) 150–154.
[14] R.W. Cahn, M. Takemaya, J.A. Horton, C.T. Liu, Mater Res. 6 (1991) 57–70.
[15] S. Nakashima, K. Takashima, J. Harase, Metall. Mater. Trans. A 28 (1997) 681–687.

[16] R. Machado, A.H. Kasama, A.M. Jorge, C.S. Kiminami, W.J. Botta, C. Bolfarini, Mater. Sci. Eng. A 449 (2007) 854–857.

[17] M. Komatsubara, K. Sadahiro, O. Kondo, T. Takamiya, A. Honda, J. Magn. Magn. Mater. 242 (2002) 212–215.

[18] T. Ros, Y. Houbaert, O. Fischer, J. Schneider, IEEE Trans. Magn. 37 (2001) 2321–2324.

[19] T. Ros-Yanez, Y. Houbaert, O. Fischer, J. Schneider, J. Mater. Process. Technol. 143 (2003) 916–921.

[20] J. Li, I. Baker, Mater. Sci. Eng. A 392 (2005) 8–22.

[21] W. Zhang, G.L. Chen, G. Chen, Mater. Sci. Eng. A 422 (2006) 241–251.

[22] Z.W. Zhang, G. Chen, H. Bei, F. Ye, G.L. Chen, C.T. Liu, Appl. Phys. Lett. 93 (2008) 191908–191911.

[23] K. Okada, T. Yamaji, K. Kasai, ISIJ Int. 36 (6) (1996) 706–713.

[24] T. Ros-Yañez, Y. Houbaert, O. Schneeweiss, J. Asensio, M. Prado, Rev. Metal. (Madrid) 36 (2000) 339–347.